Stopping power calculation of rubidium and strontium for protons

Juan Carlos Moreno-Marín [a,*], Isabel Abril [a], Rafael Garcia-Molina [b]

[a] *Departament de Física Aplicada, Universitat d'Alacant, Apartat 99, E-03080 Alacant, Spain*
[b] *Departamento de Física, Universidad de Murcia, Apartado 4021, E-30080 Murcia, Spain*

Abstract

We have evaluated the stopping cross-section (SCS) and the energy-loss straggling of rubidium and strontium targets, for a wide range of proton energies. The calculations are done in the framework of the dielectric formalism, using a combination of Mermin-type energy-loss functions to describe the behaviour of the outer electrons of the target, while the inner-shell electrons are described through their generalized oscillator strengths. Our calculated SCSs agree with the experimental data better than other theoretical and interpolated results, in a wide range of proton energies. © 2002 Elsevier Science B.V. All rights reserved.

Keywords: Stopping power; Proton energy loss; Dielectric properties of solids

Despite the importance of the stopping power of solids for basic and technological research, until now measurements of the stopping power for protons only exist in less than half of the elemental targets. To obtain information for all the other elements some interpolation in the target atomic number is necessary. Eppacher et al. [1] did measurements of the stopping power of rubidium and strontium for protons in order to check the quality of the several available interpolations [2–4], and they found differences up to 30% between interpolated data and their measurements.

In this paper we shall calculate the stopping power of rubidium and strontium for protons and compare them with experimental data as well as with interpolations and other theoretical models. Our model is based in the dielectric formalism, where the electrical properties of the target are described by a sum of Mermin-type energy-loss functions (ELFs) for the outer electron excitations of the target while the inner-shell electron excitations are described by the generalized oscillator strengths (GOSs) in the hydrogenic approach.

We assume that electronic energy loss and nuclear energy loss are not correlated and in the range of energies we shall consider we neglect the nuclear stopping [5]. Except where otherwise stated, in what follows we shall use atomic units: $m = e = \hbar = 1$ (where m and e are, respectively, the electron mass and the elementary charge; $\hbar$ is Planck's constant divided by 2π).

The electronic energy loss for a proton moving with velocity v through a target is characterized by the stopping power, S_p, and the energy-loss straggling, Ω^2. Within the framework of the (linear

---

* Corresponding author.
  E-mail address: jc.moreno@ua.es (J.C. Moreno-Marín).

response) dielectric theory, these magnitudes can be written as [6]

$$S_p(v) = \frac{2}{\pi v^2} \int_0^\infty \frac{dk}{k} \int_0^{kv} d\omega\, \omega\, \text{Im}\left[\frac{-1}{\epsilon(k,\omega)}\right], \qquad (1)$$

$$\Omega^2(v) = \frac{2}{\pi v^2} \int_0^\infty \frac{dk}{k} \int_0^{kv} d\omega\, \omega^2\, \text{Im}\left[\frac{-1}{\epsilon(k,\omega)}\right]. \qquad (2)$$

k and ω are, respectively, the momentum and the energy transferred to electronic excitations of the target and $\epsilon(k,\omega)$ is the longitudinal dielectric function of the target.

We describe the dielectric properties of real targets using a linear combination of Mermin-type ELFs, $\text{Im}(-1/\epsilon_M)$, for outer electron excitations [7–9]. The Mermin dielectric function [10], which is a generalization of the Lindhard dielectric function [6], provides a more realistic description of the dielectric properties of the target, because it includes dissipation effects that happen in real solids besides to preserve the local number of electrons in the target. Our procedure consists in fitting the ELF to the experimental energy-loss spectrum obtained in the optical limit, $k = 0$, for a wide range of transferred energies, that is,

$$\text{Im}\left[\frac{-1}{\epsilon(k=0,\omega)}\right]_{\text{exper(outer)}}$$
$$= \sum_j A_j\, \text{Im}\left[\frac{-1}{\epsilon_M(k=0,\omega;\omega_j,\gamma_j)}\right], \qquad (3)$$

where the parameters A_j, ω_j and γ_j, are related to the intensity, the position and the width, respectively, of the peaks and other structures observed in the energy spectrum.

The description of the inner-shell electron excitations is given by a single-atom model through the GOS; this model is appropriate because the inner-shell electrons have large binding energies and show negligible collective effects. The relation between the dielectric ELF and the GOS is given by [11]

$$\text{Im}\left[\frac{-1}{\epsilon(k,\omega)}\right] = \frac{\pi\omega_{p0}^2}{2\omega}\frac{df(k,\omega)}{d\omega}, \qquad (4)$$

where $df(k,\omega)/d\omega$ is the GOS per unit excitation energy and ω_{p0} is the plasmon energy corre-

sponding to one free electron per atom. We use the GOS in the hydrogenic approach because it gives realistic values of the inner-shell ionization cross-sections [12] and provides analytical expressions for K and L shell ionization [13–15].

The constructed ELF must also verify the *f*-sum rule for the effective number of electrons in the target,

$$N_{\text{eff}}(\omega) = \frac{1}{2\pi^2 n} \int_0^\omega d\omega'\, \omega'\, \text{Im}\left[\frac{-1}{\epsilon(k,\omega')}\right], \qquad (5)$$

where n is the atomic density of the material and N_{eff} is the effective number of electrons participating in electronic excitations up to a given energy ω. In the limit of high energy transfer ($\omega \to \infty$) all the electrons of the atom can be excited and N_{eff} will be equal to the total number of target electrons. Note that Mermin dielectric functions safeguard the verification of the *f*-sum rule for all momentum transferred, k, if it is satisfied for $k = 0$.

The construction of the ELF of rubidium and strontium requires the availability of the corresponding experimental excitation spectra at $k = 0$ in a wide range of energies, which unfortunately is not possible. For rubidium we do not know any experimental data of the ELF at low transfer energies ω, therefore we shall use ab initio calculations of the energy-loss spectra made by Aryasetiawan and Karlsson [16] along the (1 1 0) direction within the random phase approximation, which include band structure effects, core electrons and local field effects. They found in the ELF of rubidium a maximum at ~4 eV corresponding to plasmon excitations and a shoulder structure at ~7 eV, which arises from interband transitions to the d band. These calculations were made at different values of the momentum transfer, k (but not at $k = 0$).

For strontium target there are experimental data of the energy-loss spectra from Langkowski [17], in the range of 2–50 eV, obtained from transmission electron energy-loss experiments. The error of this determination is estimated to be about 10–20% caused by the uncertainty in the intensity measurements of the energy-loss spectrum and by the separation of the intensity of strontium and the substrate. The structure of the ELF of

strontium shows a small peak at ~4 eV as a result of interband transitions, the losses at ~8 eV are due to the bulk plasmon and the higher energetic losses at ~29 eV correspond to collective contribution to the interband transitions.

The ELF of rubidium and strontium for $\hbar\omega$ greater than a few tens of eV can be obtained from the Henke model based in the X-ray scattering factors [18,19]. Although the results obtained would not be reliable for energies corresponding to the excitation of the valence electrons, they are usually correct for energies comparable to that of the inner shells.

In Fig. 1(a) and (b) (left axes) we present the ELF at $k = 0$ of rubidium and strontium, respectively. The ELF we will use, obtained through the

fitting with Eq. (3) for the outer electron (M, N and O shells) excitations and by the GOS for the inner electrons (K and L shells), is shown by a solid line. The parameters used in our fitting of the ELF for the outer electrons are given in Table 1. In Fig. 1(a) we also represent by a dotted line the rubidium ELF calculated by Aryasetiawan and Karlsson [16] for low excitation energies, and open symbols correspond to the ELF obtained from the X-ray scattering factors [18,19]. In Fig. 1(b) we also display by symbols the experimental ELF of strontium from Langkowski [17] for low excitation energies and the ELF obtained from the X-ray scattering factors [18,19] for high excitation energies. Note that the absence of experimental data for the ELF at intermediate excitation energies makes difficult to connect the low and high energy regions of the ELF because at these intermediate energies it is not clear whether the X-ray scattering factors work. The right axes of Fig. 1(a) and (b) correspond to the effective number of electrons that participate in electronic excitations at a given energy, Eq. (5). It can be seen how the inner-shell electrons contribute progressively to N_{eff} as the excitation energy ω increases, and tend to the total number of electrons when $\omega \to \infty$, verifying the *f*-sum rule.

As an additional checking to our calculations we have evaluated also the mean excitation energy *I* of rubidium and strontium targets [20],

$$\ln I = \frac{1}{2\pi^2 n N_{tot}} \int_0^\infty d\omega\, \omega \ln \omega\, \mathrm{Im}\left[\frac{-1}{\epsilon(k,\omega)}\right], \qquad (6)$$

where N_{tot} is the total number of electrons of the atom. We obtain $I(\mathrm{Rb}) = 298$ eV and $I(\mathrm{Sr}) =$
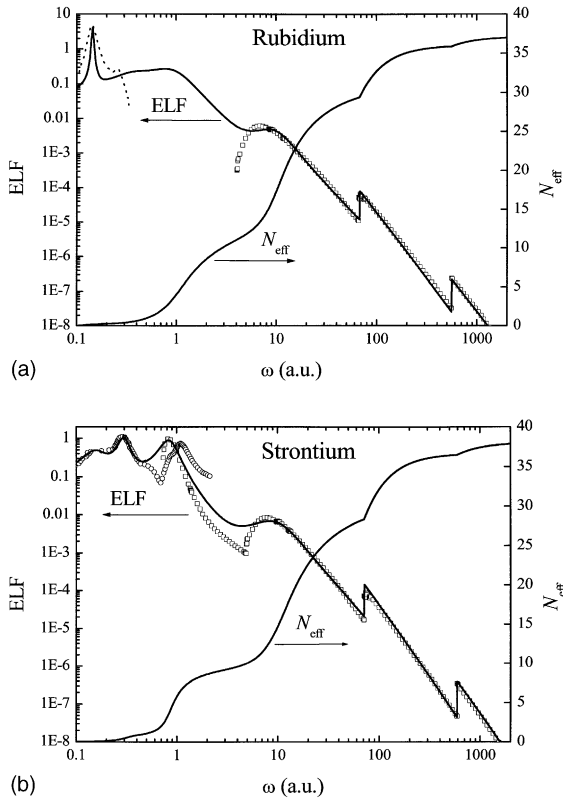

(a)

(b)

Fig. 1. ELF at $k = 0$ (left axes) and effective number of electrons (right axes) of (a) rubidium and (b) strontium as a function of the excitation energy. Solid lines represent our fitting to the ELF, dotted line is the calculated ELF from [16] and symbols are (○) from [17] and (□) from [18,19].

Table 1
Parameters used to fit, through Eq. (3), the optical ELF of Rb and Sr

Target	j	ω_j (a.u.)	γ_j (a.u.)	A_j
Rb	1	0.144	0.006	1.93×10^{-1}
($\rho = 1.53$ g/cm^3)	2	0.4	0.4	9.38×10^{-2}
	3	0.95	1.06	2.64×10^{-1}
	4	9.7	9.0	3.89×10^{-3}
Sr	1	0.16	0.1	2.34×10^{-1}
($\rho = 2.54$ g/cm^3)	2	0.3	0.09	2.78×10^{-1}
	3	0.84	0.383	4.07×10^{-1}
	4	10.0	11.0	6.70×10^{-3}

374 eV while interpolations [21] give $I^{int}(Rb) = 363$ eV and $I^{int}(Sr) = 366$ eV. For strontium target the difference between the mean excitation energy obtained with our model and the interpolated values is $\sim$2% whereas for rubidium target is $\sim$20%. In order to elucidate this discrepancy, experimental data of the rubidium ELF are necessary, specially at low and intermediate excitation energies.

Using the previous representations of the ELF for rubidium and strontium, we have calculated the corresponding stopping power and energy-loss straggling for protons by integrating their ELFs over the k–ω plane, as indicated by Eqs. (1) and (2). Dividing the stopping power of each material by the corresponding atomic density we obtain the stopping cross-section (SCS) of rubidium and strontium, which are shown as solid lines in Fig. 2(a) and (b), respectively. Our results are compared with experimental data from Eppacher et al. [1], and with semiempirical predictions of SRIM [22]. A detailed discussion on the differences between experimental data and several interpolations [2–4] was made by Eppacher et al. [1]. Calculations of the SCS based in an uniform free electron gas approximation using the Lindhard dielectric function [6] are also depicted, where a plasmon frequency $\omega_p = 0.143$ a.u. for rubidium and 0.254 a.u. for strontium was utilized. We also display in Fig. 2(a) and (b) the SCS obtained by the density functional theory valid for low-energy protons [23]; in this model a non-linear calculation of the transport cross-sections and friction coefficients was considered.

As can be observed in Fig. 2(a), our calculation of the rubidium SCS agrees roughly with the experimental data [1], although it overestimates $\sim$5% the experimental values at high proton energies; at low energies, where there are not experimental data, the agreement with the model based in the density functional theory [23] is good. Perhaps the differences existing between the calculated and the experimental SCS could be due to the lack of experimental data of the rubidium ELF. The SCS obtained by the SRIM code [22] give the correct value of the proton energy at the maximum SCS, but they underestimate the height of the maximum SCS in $\sim$10% with respect to experimental data.
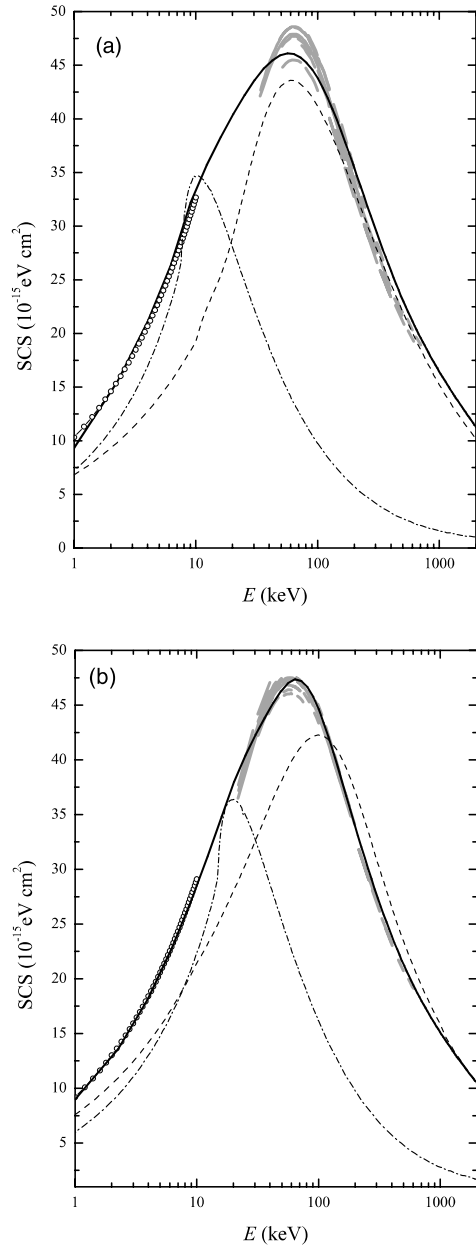

Fig. 2. SCS of (a) rubidium and (b) strontium as a function of the proton energy. The solid lines represent our calculations, the very thick grey solid lines refer to experimental data fom Eppacher et al. [1]; the dashed lines are the prediction of SRIM [22]; the dot-dashed lines correspond to the free electron gas approximation [6] and the open circles are the results from the density functional theory [23].
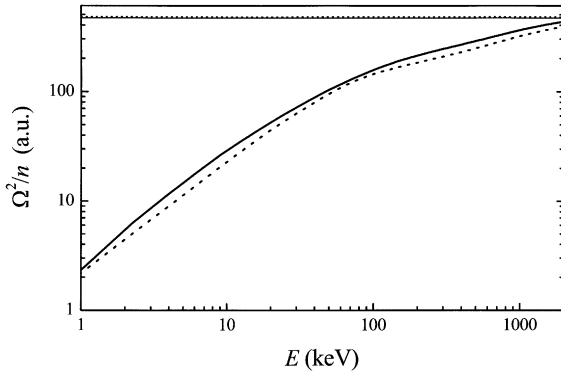
Fig. 3. Normalized energy-loss straggling, Ω^2/n, of rubidium (—) and strontium (- - -) as a function of the proton energy. The thin horizontal lines represent the corresponding Bohr limit at high energies.

The uniform free electron gas model clearly disagrees with the experimental values.

Our calculation of the strontium SCS shown in Fig. 2(b) compares very well with the experimental data in all the range of proton energies. Besides, at low proton energies, where there is not available experimental data, our results compare well with the predictions of the density functional theory [23] where a stopping power proportional to the projectile velocity is obtained. In this case the SRIM [22] values of the SCS clearly disagree with the experimental data, because they do not reproduce neither the correct position nor the height of the maximum SCS. Again, the model based in the free electron gas does not agree with experimental data, in both cases, rubidium and strontium because the maximum SCSs are displaced to low proton energies and their magnitudes are much smaller than the experimental values.

In Fig. 3 we show the normalized energy-loss straggling, Ω^2/n, of rubidium (solid line) and strontium (dashed line) as a function of the proton energy. At low proton energies we obtain that the energy-loss straggling is proportional to the proton velocity and at high proton energies we reproduce the Bohr's energy-loss straggling [24], which gives the high-energy limit: $\Omega_{\mathrm{B}}^2/n = 4\pi Z_1^2 Z_2 e^4$, where Z_1 and Z_2 are, respectively, the atomic number of the projectile and the target atoms.

In conclusion, we have been presented a model to evaluate the proton electronic energy loss based in the dielectric formalism, where the dielectric properties of the target are described by a sum of Mermin-type ELFs for the outer electrons combined with a GOS description for the inner-shell electrons. Our results of the SCS of rubidium and strontium agree better than the interpolated values with available experimental data in a wide range of proton energies.

Acknowledgements

References

[1] Ch. Eppacher, G. Zemsauer, D. Semrad, Nucl. Instr. and Meth. B 90 (1994) 92.

[2] H.H. Andersen, J.F. Ziegler, in: The Stopping and Ranges of Ions in Matter, Vol. 3, Pergamon, New York, 1977.

[3] J.F. Janni, At. Data Nucl. Data Tables 27 (2–5) (1982).

[4] J.F. Ziegler, J.P. Biersak, U. Littmark, in: The Stopping and Ranges of Ions in Matter, Vol. 1, Plenum, New York, 1985.

[5] H.E. Schiott, Mat. Fys. Medd. Dan. Vid. Selsk 35 (9) (1966).

[6] J. Lindhard, K. Dan. Vidensk. Selsk., Mat. -Fys. Medd. 28 (8) (1954).

[7] I. Abril, R. Garcia-Molina, N.R. Arista, Nucl. Instr. and Meth. B 90 (1994) 72.

[8] D.J. Planes, R. Garcia-Molina, I. Abril, N.R. Arista, J. Electr. Spectrosc. Related Phenom. 82 (1996) 23.

[9] I. Abril, R. Garcia-Molina, C.D. Denton, F.J. Pérez-Pérez, N.R. Arista, Phys. Rev. A 58 (1998) 357.

[10] N.D. Mermin, Phys. Rev. B 1 (1970) 2362.

[11] U. Fano, Ann. Rev. Nucl. Sci. 13 (1963) 1.

[12] R.F. Egerton, Electron Energy-Loss Spectroscopy in the Electron Microscope, Plenum Press, New York, 1989.

[13] D.H. Madison, E. Merzbacher, in: B. Crasemann (Ed.), Theory of Charged-Particle Excitation, Atomic Inner-Shell Processes, Vol. 1, Academic Press, New York, 1975, p. 1.

[14] M.C. Walske, Phys. Rev. 101 (1956) 940.

[15] B.H. Choi, E. Merzbacher, G.S. Khandelwal, At. Data 5 (1973) 291.

[16] F. Aryasetiawan, K. Karlsson, Phys. Rev. Lett. 73 (1994) 1679.

[17] J. Langkowski, J. Phys. D: Appl. Phys. 8 (1975) 2058.

[18] B.L. Henke, E.M. Gullikson, J.C. Davis, At. Data Nucl. Data Tab. 54 (2) (1993) (The ASCII files for the scattering factors of the different elements can be obtained from http://xray.uu.se/hypertext/henke.html).

[19] E.D. Palik, G. Ghosh, Electronic Handbook of Optical Constants of Solids, Academic Press, San Diego, 1999.

[20] E. Shiles, T. Sasaki, M. Inokuti, D.Y. Smith, Phys. Rev. B 22 (1980) 1612.

[21] ICRU Report 49, Stopping Powers and Ranges for Protons and Alpha Particles, International Commission for Radiation Units and Measurements, Bethesda, 1992.

[22] J.F. Ziegler, SRIM. The Stopping and Range of Ions in Matter, Version 2000.

[23] J. Calera-Rubio, A. Gras-Martí, N.R. Arista, Nucl. Instr. Meth. B 93 (1994) 137;
J. Calera-Rubio, private communication.

[24] N. Bohr, K. Dan. Vidensk. Selsk, Mat. Fys. Medd. 18 (8) (1948).